Indian Ocean Dynamic Sea Level, Variability And Projections In CMIP6 Models

Abhisek Chatterjee (chatterjeea.ocean@gmail.com)
Indian National Center for Ocean Information Services https://orcid.org/0000-0001-5529-7997
Sajidh C K
Indian National Center for Ocean Information Services

Research Article

Keywords: Ocean dynamics, Climate modes, Indian Ocean Dipole, Global warming, Emission scenarios

Posted Date: January 3rd, 2022

DOI: https://doi.org/10.21203/rs.3.rs-1192038/v1

Indian Ocean dynamic sea level, variability and projections in CMIP6 models

Sajidh C K and Abhisek Chatterjee*

Indian National Centre for Ocean Information Services, Hyderabad, India

* e-mail: abhisek.c@incois.gov.in

Abstract

The regional sea level variability and its projection amidst the global sea level rise is one of the major concerns for coastal communities. The dynamic sea level plays a major role in the observed spatial deviations in regional sea level rise from the global mean. The present study evaluates 27 climate model simulations from the sixth phase of the coupled model intercomparison project (CMIP6) for their representation of the historical mean states, variability and future projections for the Indian Ocean. Most models reproduce the observed mean state of the dynamic sea level realistically, however consistent positive bias is evident across the latitudinal range of the Indian Ocean. The strongest sea level bias is seen along the Antarctic Circumpolar Current (ACC) regime owing to the stronger than observed south Indian Ocean westerlies and its equatorward bias. Further, this equatorward shift of the wind field resulted in stronger positive windstress curl across the southeasterly trade winds in the southern tropical basin and easterly wind bias along the equatorial waveguide. These anomalous eastlerly equatorial winds cause upwelling in the eastern part of the basin and keeps the thermocline shallower in the model than observed, resulted in enhanced variability for the dipole zonal mode or Indian Ocean dipole in the tropics. In the north Indian Ocean, the summer monsoon winds are weak in the model causing weaker upwelling and positive sea level bias along the western Arabian Sea. The high-resolution models compare better in simulating the sea level variability, particularly in the eddy dominated regions like the ACC regime in interannual timescale. However, these improved variabilities do not necessarily produce a better mean state likely due to the enhanced mixing driven by parametrizations set in these high-resolution models. Finally, the overall pattern of the projected dynamic sea level rise is found to be similar for the mid (SSP2-4.5) and high-end (SSP5-8.5) scenarios, except that the magnitude is higher under the high emission situation. Notably, the projected dynamic sea level change is found to be milder when only the best performing models are used compared to the full ensemble.

Keywords: Ocean dynamics, Climate modes, Indian Ocean Dipole, Global warming, Emission scenarios

1. Introduction

The ongoing global warming owing to the increase in the concentration of anthropogenic greenhouse gasses causing a devastating irreversible impact on the global climate systems (IPCC AR6, 2021). About 93% of the extra heat stored in the climate system is absorbed by the ocean, leading to a rapid sea level rise in the recent decade and therefore, posing a great threat to the densely populated low-lying coastal areas across the globe (Oppenheimer et al., 2019). As per the latest report of the IPCC (Intergovernmental Panel on Climate Change; IPCC AR6, 2021) the global mean sea level has increased at a rate of 1.8 mm/yr (Meehl et al., 2007). However, availability of the altimeter observation over the last few decades indicates a much rapid increase of global sea level rise at a rate

of ~3.2 mm/yr (Bindoff et al., 2007; Han et al., 2010; Church and White, 2011; Church et al., 2013; Unnikrishnan et al., 2015). The rising rate further increased to 3.6 mm/yr during the period 2005-2015 (IPCC AR6, 2021), suggesting a nearly two-fold increase in the global sea level rise in the early part of the 21st century. This rising sea level is expected to increase further at a rapid pace unless a deep reduction in CO_2 emission becomes a reality across the globe (Perrette et al., 2013; Oppenheimer et al., 2019). Moreover, this higher sea level along with warmer climate is expected to exacerbate extreme weather events such as storm surges, cyclones, high waves and greater erosion which will put human lives at the risk of coastal calamities around the globe, particularly in the heavily populated south Asian countries where these effects will be devastating.

More importantly, the regional sea level change differs significantly from the global mean driven by local wind, ocean dynamics, differential heating and gravitational and solid earth processes (Lowe and Gregory 2006; Christensen et al., 2007; Milne et al., 2009; Yin et al., 2010, 2012; Meyssignac et al. 2012; McGregor et al. 2012; Landerer et al., 2007, 2014). Moreover, this non-uniform change of sea level is also the manifestation of both the internal variability as well as the anthropogenic forcing (Han et al., 2010). While the contribution of natural internal variability is one of the dominating forcing in the interannual/decadal timescale, the contribution of the anthropogenic component is expected to be the primary cause in the warmer future (Stammer et al., 2013). The internal variability in the Indian ocean is associated with coupled climate modes such as El Nino Southern Oscillation (ENSO), Indian Ocean Dipole (IOD), Pacific decadal Oscillation (PDO), Southern Annular Mode (SAM), etc. (Phillips et al., (2021) and the references therein). Therefore, at a local level, for the policymakers, the global mean assessments are of little use. In order to build and implement mitigation policies against the climate change risks, the regional assessment of sea level rise and associated extremes are more important than the global mean (Cazenave and Cozannet, 2014).

Phase six of the Coupled Model Inter-comparison Project (CMIP6), like its predecessors, brings standardized model outputs of the historical simulations as well as the future projections of the groups participating in the project (Eyring et al., 2015), allowing a detailed regional specific investigation of the sea level change and associated processes. The model simulated dynamic sea level (DSL) represents the change in sea level due to the thermal and halosteric changes along with dynamic processes associated with wind forcings (Stammer et al., 2013). The mean state simulation of sea level from CMIP3 to CMIP5 has shown a marked improvement while there has been no considerable change from CMIP5 to CMIP6, but the zonal wind stress representation has slightly improved from CMIP5 to CMIP6. The CMIP6 models report increased DSL projections compared to CMIP5 models, which many linked to the inclusion of models with higher climate sensitivity (Andrews et al., 2012; Lyu et al., 2020; Brunner et al., 2020; Nijsse et al., 2020; Tokarska et al., 2020; Hermans et al., 2021). While, in the CMIP5, the future projections were driven by different climate scenarios based on the representative concentration pathways (RCPs) associated with varied radiative forcing ranging from 2.6 to 8.5 Wm^{-2} (Van Vuuren et al., 2011), In the CMIP6 models a new set of future climate scenarios are adopted based on the Shared Socioeconomic Pathway (SSP) which additionally considers land use, urbanization, economy, population, etc. (O'Neill et al., 2016; Riahi et al., 2017). Therefore, the narrative of the projected changes under the CMIP6 scenarios are similar to the CMIP5 scenarios, but not the same. We expect that the projected regional change in sea level and its variability may differ significantly under these new SSP considerations compared to the previous estimates.

Notably, proper mean state representation is an important requisite for models simulating future projections (Ritcher et al., 2017). Along with mean state simulations, an accurate representation of internal variability is also imperative for better projections. However, the ensemble spread of the

climate models increases the uncertainty of the projected change. To reduce this uncertainty the performance backed weightage or exclusion of models has been explored in many previous studies (Greene et al. 2006; Yin et al., 2010; Watterson and Whetton 2011). Most of these assessment studies for different variables and regions employed subjective ranking of models based on their ability to simulate large scale climate patterns and skill score metrics (Mcsweeny et al.,2015; Halder et al.,2020; Krishnan and Bhaskaran, 2019). McSweeney et al. (2015) provided a rationale that the inability of the model to simulate key large-scale processes may reflect in the model's deficiency in simulating climate signals induced by global warming. Nevertheless, finding a selection rationale that suits best for the proposed purpose is a challenging task. Note, however, that while such exclusion of non-performing models for the ensemble projection reduces the uncertainty and narrow down the projected spread, it also increases the risk of mal-adaptation (McSweeney et al., 2015). However, as the cost of implementing mitigation policies to safeguard a coast from rising sea level is expected to increase exponentially with the projected future sea level rise, lowering the uncertainty is likely to provide a sustainable solution. Further, as the oceanographic operational centres across the globe are more interested in downscaling the global sea level rise using a dynamical and statistical approach, the requirement of selected best performing models for the region of interest is needed for such analysis.

In this study, we analyse historical sea level simulations from CMIP6 models to identify their fidelity in simulating the observed mean state and variability of the Indian Ocean. Further, we select a subset of models based on their performance for various climatic features of the Indian Ocean. We expect that the exclusion of such least-performing models from the ensemble may likely provide policy-relevant projections over the Indian ocean domain. Further, considering the different driving dynamical mechanisms responsible for mean sea level and its variability, we discussed the model biases and their underlying mechanisms separately for the north Indian Ocean (NIO; 0^{o}-30^{o}N), south tropical Indian Ocean (STIO; 0^{o}-30^{o}S) and Southern Indian Ocean (SIO; 30^{o}S-60^{o}S). The rest of the paper is organized as follows: Section 2 described the observation and models we use in this study, the mean sea level, its variability, biases and projected change are discussed in Section 3 and finally, in section 4 we conclude our results.

2. Data and Methodology

In this study, we use outputs from 27 CMIP6 models (Eyring et al., 2016; Table 1). To assess the fidelity of each model in reproducing the Indian Ocean mean state and its variability the 'historical' simulation (available from 1850 to 2014) of sea surface height above geoid (zos), downward zonal and meridional windstress at the surface (tauu, tauv), and derived curl of the windstress are analysed. For future projections, we analyse two Shared Socioeconomic Pathways (SSP) scenarios from Scenario Model Intercomparison Project (ScenarioMIP; O'Neill et al., 2016) for a possible mid-emission (SSP2-4.5) and high-emission (SSP5-8.5) radiative forcing at the end of 2100. To give equal weightage to all the models only the first realization 'r1i1p1f1' is used for both historical and future scenarios. The dynamic sea level (DSL) is defined as the *zos* after removing the global mean at each time step (Gregory et al.,2019). This treatment is necessary to compare each model with the observed satellite altimeter derived SSH as the global mean is zero at each time step. We apply the inverse barometer effect corrections due to sea ice for those models for which this correction is not already applied such as GISS-E2-1-G (Griffies et.al 2016). Also, to treat the sea ice mass per area of the model is converted into the height it would occupy as water and is added to the model sea surface

height. Finally, all the model variables are re-gridded onto a uniform $1^o \times 1^o$ grid for ease of comparison and to compute the multi-model mean (MMM) of these models.

Owing to the limitation of observational data for sea surface height the multi-mission gridded altimeter derived sea surface height from the year 1993-2014 is used. In order to compare the model derived DSL with the altimeter we remove the time-dependent global mean from the observation as well. As the altimeter-derived sea level is found to have a correlation greater than 0.98 with the mean dynamic topography (Maximenko et al.,2019; Lyu et al., 2020a), the use of altimeter sea level anomaly does not affect our analysis. As the altimeter sea level observation is available only for a shorter duration, the variability may be biased by the unresolved decadal climate variability. Moreover, the phase of the model simulations is also expected to differ from the altimeter for such a short time period. Hence, to assess the model simulated variability, we use a 20-year sliding window on the entire available record from the model simulations.

Since the DSL is primarily influenced by dynamical forcing, we also analyze the windstress field for each of the CMIP6 models. Windstress curl is derived from the models for historical and future scenario simulations as it is one of the primary drivers of the mean dynamic sea level and its variability in the interior ocean. To compare the wind field and its anomaly, we use European Centre for Medium Range Weather Forecasts (ECMWF) Reanalysis (ERA5) dataset for the period 1979 to 2014 (Hersbach and Dee, 2016).

In order to assess the performance of each model, basic statistical metrics such as pattern correlation, root mean square error, Empirical Orthogonal Function (EOF), etc. are used. We also use a skill score metric defined by Taylor (2001) as given below:

$$S = \frac{4 + (1 + R)}{(\sigma + \frac{1}{\sigma})^2 (1 + Ro)} \quad (1)$$

$\sigma \left(= \frac{\sigma_m}{\sigma_o}\right)$ is the ratio of the standard deviation of the model (σ_m) and observation (σ_o). Ro the maximum attainable correlation and is set to 1. The standard deviation is calculated on the detrended sea level at each point in time for a specific frequency band. The skill score is repeated for each of the 20-year sliding windows to assess how each model captures the observed variability.

3. Results

3.1 Mean dynamic sea level

The mean DSL represents the annual geostrophic circulation driven by the overlying windstress and windstress curl of the basin and therefore, plays a key role in the redistribution of heat and mass across the basin. While in the SIO the DSL is primarily driven by the semi-permanent mid-latitude Southern Ocean westerlies, in the STIO it is driven by the southeasterly trade winds. On the other hand, DSL in the NIO is driven by the seasonally reversing monsoon winds which reverse from southwesterly in the boreal summer to the northeasterly in the boreal winter. Hence, in the NIO the sign of the DSL also reverses with the season. However, as the winds are much stronger during the boreal summer, the annual mean DSL and winds are biased towards the summer monsoon season of the NIO (Figure 1).

All the CMIP6 models could reproduce the mean DSL and wind field reasonably well across the basin. Notably, while the multi-model-mean (MMM) could capture the mean sea level patterns very well, there is a consistent positive bias in the zonally averaged sea level across the basin for most of the models (Figure 2a). The strongest positive sea level bias is evident across the Antarctic circumpolar current (ACC) regime in the SIO (Figure 1). This region is driven by strong westerlies causing a marked shift in the sign of the windstress curl across the wind field maxima (Figure 2b, c). In response to the winds, the sign of DSL across the Antarctic circumpolar current (ACC) regime also shifts from negative in the south of ACC to positive in the north of ACC. Note here that most climate models tend to simulate an equatorward bias in the westerly wind field causing an equatorward shift in the ACC regime relative to the observation (Fyfe and Saenko 2006; Russell et al. 2006; Lyu et al., 2020a, 2020b). While this equatorward westerly wind bias is reduced considerably in the 6th phase of the CMIP models compared to its predecessors (Lyu et al., 2020a), it is still off by ~1^{o} in the MMM in the Indian Ocean sector of the mid-latitude Southern Ocean basin. In fact, ~63% models (17 model out of total 27) produced such equatorward bias in the westerlies in the SIO which is slightly larger than the global mean reported earlier by Lyu et al. (2020a). This strong wind bias also causes a very strong negative (positive) windstress curl bias in the south (north) of the zero windstress curl region (Figure 2c), causing a sharp change in the DSL compared to the observation. In the STIO, particularly in the western part, the model simulated sea level is slightly higher compared to the observation mainly linked to the stronger southeasterly trade winds in the model. However, in the NIO, weaker model simulated summer monsoon winds (Figure 1 and S1) produce weak upwelling along the coast of Somalia and Arabia, causing a positive bias in the model simulated mean sea level in the western Arabian Sea (Figure 1c). This also led to a contrasting east-west bias in the sea level across the NIO in most models.

The performance of the individual models differs considerably in the various latitude bands. Figure 3 shows the spread of the sea level bias of the individual CMIP6 models for the NIO, STIO and SIO. Overall, the bias is more in the western part of the basin due to boundary currents and instabilities across all latitudes. Also, bias generally increases from north to south. While in the NIO most models show RMSE (with respect to altimeter) less than 0.15 m except for the INM-CM5-0; in the SIO the RMSE is predominantly more than 0.15 m and reaches close to 0.3 m for the NorESM2-LM. The RMSE for the MMM in the NIO, STIO and SIO are 0.9 m, 0.12 m and 0.16 m, respectively.

3.2 Variability

In this section, we analyze the ability of the CMIP6 models to simulate the key variability features in the Indian ocean domain. The sea level over the Indian Ocean shows strong variability in a large spectrum of timescale. While the variability in the seasonal timescale is most prominent due to the dominance of the seasonally reversing monsoon winds in the north Indian Ocean (Chatterjee et al., 2012), the variability in the interannual and decadal timescale is of key importance for the Indian Ocean climate variability and its impact on the global climate (Schott et al., 2009; Phillips et al., 2021).

Observed variability of the Indian Ocean shows maxima along the front of the ACC in the SIO (Figure 4a) owing to the interannual meridional movement of the ACC current regime (Figure 4g) driven by ENSO and SAM climate modes (Kim and Orsi, 2014). The thermocline ridge region of the STIO also exhibits stronger variability primarily influenced by the South Equatorial Current (SEC) and the associated embedded eddies in seasonal and interannual timescale (Wang et al., 2021; Deepa

et al., 2021). The region off the west coast of Australia in the latitude band of 15°S-35°S also show strong interannual variability (Figure 4g) driven by the eddies generated due to the baroclinic instabilities between the surface eastward flowing South Indian Counter Current (SICC) and subsurface westward flowing SEC (Jia et al., 2011; Menezes et al., 2014; Zhang et al., 2020). In the NIO, the western boundary of the Arabian Sea along the coast of Somalia and Arabia shows strong variability in seasonal and interannual timescale driven by the summer monsoon winds and its climate variability (Beal and Donohue, 2013; Chatterjee et al., 2019; Lakshmi et al., 2020; Vinayachandran et al., 2021). Also, coastal waveguide along the perimeter of the Bay of Bengal exhibits significant variability driven by coastal propagation of planetary waves forced by the equatorial winds (Vialard et al., 2009; Suresh et al., 2012; Chatterjee et al., 2017; Mukherjee et al., 2017; Phillips et al., 2021).

The historical simulations of CMIP6 models are evaluated for the Indian Ocean variability for the common period of data availability from altimeter and CMIP6 models i.e. during 1993-2014 (Figure 4b,e,h and Figure S2). Most of the CMIP6 models underestimate the Indian Ocean variability. This also reflects in the weaker variability of the MMM across the Indian Ocean basin (Figure 4b). Nevertheless, models perform relatively well for the seasonal scale with almost accurate representation in the variability associated with the Great Whirl fronts in the western Arabian Sea, its extension along the summer monsoon currents and along the perimeter of the Bay of Bengal (Figure 4e). Models produce much stronger variability in the eastern equatorial Indian Ocean and along the coast of Java, likely due to the shallow mixed layer leading to stronger air-sea momentum exchange in the upper water column and hence, anomalously stronger excitation of lower-order baroclinic modes. In the interannual timescale, models severely underperformed in simulating variability along the fronts of the ACC current regime. The weaker variability is noticed for the STIO along the band of the SICC regime as well. Notably, the high-resolution models like CMCC-CM2-HR4, CNRM-CM6-1-HR, HADGEM3-GC31-MM and MPI-ESM1-2-HR performed relatively better in reproducing this observed variability, particularly along the ACC current regime. This indicates that the eddy dominated regions are simulated well by the high-resolution models compared to the course CMIP6 models. As this eddy induced high-frequency variability cause strong low-frequency rectification through modifying the mean state and therefore, impacting the response of climate modes and the internal variability, the natural variability of the Indian Ocean is likely underestimated in most CMIP6 models. For the thermocline ridge region, the variability in MMM is more spread out compared to the observation with a decrease in the magnitude of the variability eastwards. The CMCC models capture the eastward variability properly but overestimate in the west. On the other hand, the high-resolution CNRM model does capture the variability pattern, but the simulated magnitude of the variability is lower than the observation. The HadGEM3-GC31-MM model fare better compared to others in simulating the observed location and magnitude of the variability in this region (Figure S2).

Notably, the phase and magnitude of the internal variability in the model may differ with observation due to freely evolving internal variability in the system. Therefore, one can expect the model simulated variability to differ considerably during a given period (Richter et al., 2017). In order to account for the contribution of internal variability, pattern correlation and RMSE of the model simulated sea level for a 20-year sliding window is also analysed for each model to see if choosing a specific period affects the models' skill in simulating the sea level variability (Figure 5) considerably. Interestingly, the spread of the pattern correlation and RMSE doesn't vary significantly for most models. The difference in the maximum and minimum correlation for most of the individual models is ~0.1 and for RMSE it is ~0.25 cm. Models with larger correlation values tend to have smaller RMSE. This indicates the fact that the internal variability doesn't affect the overall skill of the model in simulating the Indian Ocean variability across the decade. Nevertheless, as observed in the model

simulated special variability maps (Figure 4), most models score poorly in pattern correlation with very high RMSE. In comparison, the high-resolution models show a much superior correlation and a significantly lower RMSE.

3.3 Equatorial tilt and climate variability

Next, we compare the model simulated mean DSL for the equatorial belt. The east-west sea level gradient is an important parameter as it is dynamically linked to the depth of the thermocline and therefore, modulates the air-sea interactions over the basin. This mean state particularly become important for the initiation and progression of tropical climate modes such as El Nino, Indian Ocean Dipole, etc. (Ham and Kug, 2015; Cai and Cowan, 2013). Earlier Lyu et al (2020a) showed that the new generation CMIP6 models could not produce better results compared to the CMIP5 models in simulating the observed equatorial sea level gradient. Here, we try to assess individual models mean state and relate that to the model performance pertaining to the simulated tropical climate variability. The mean DSL is averaged over 2^{o}N-2^{o}S and the zonal mean is removed to compare with the observed sea level slope (low in the west and increasing eastward). As the equatorial slope is primarily driven by the equatorial westerlies, zonal windstress averaged over the same equatorial band is also analysed (Figure 6).

The equatorward bias of the SIO westerlies and STIO trade winds leads to unrealistic equatorial easterlies in most of the models (Figure S1) and thus in the MMM wind field (Figure 1), causing underestimation in the strength of the westerlies along the equator. Simulated bias in the equatorial sea level is consistent with the bias in the zonal wind field. The MMM sea level is primarily flat along the equator and completely failed to produce the observed slope of the sea level. In fact, 7 models show a negative pattern correlation in producing mean sea level relative to the observation with RMSE of more than 0.5. In general, the models with higher correlation show lower RMSE in equatorial sea level. Moreover, in contrast to the variability, the high-resolution models do not show any superiority over the coarser models. As the equatorial sea level is primarily forced by the equatorial winds, the skill of the zonal windstress agrees well with the sea level. However, for winds, unlike sea level, a higher positive correlation does not correspond to a lower RMSE.

Further, the anomalous equatorial easterlies in CMIP6 models cause an IOD like pattern with cooler SST in the east and warmer in the west (Figure not shown). As a result, thermocline becomes too deep in the western equatorial IO and unrealistically shallow in the eastern side in most models. Earlier Fathrio et al. (2017) noted this warmer SST and deepened thermocline in the CMIP5 model. Also, Cai and Cowan (2013) suggest that such shallow thermocline depth in the east leads to anomalously strong air-sea interactions and thereby overestimate the IOD amplitude in the models. As the CMIP6 models do not show any major improvement in simulating the equatorial sea level tilt and therefore, continue to remain biased towards the IOD like pattern in the tropical belt.

To understand how this underestimation of equatorial slopes affects the simulation of internal climate modes, we perform EOF on the detrended model simulation after removing the annual cycle and compared it with observations (Figure 7). The patterns of the first and second modes of EOF are captured fairly well by the CMIP6 models. While the MMM could capture the observed spatial patterns of the first and second modes of EOF, there is a considerable departure in explaining the spatial magnitude and variability. The first mode of EOF, which represents the dipole mode of the tropical Indian Ocean, explains about 30% in the MMM compared to the 16% of the observation. This overestimation of the variability in IOD mode is primarily linked to the anomalous equatorial

easterlies in the CMIP models which causes unrealistically shallow thermocline in the eastern equatorial IO and thereby intensify air-sea climate feedback (Cai and Cowan, 2013). The variability for the second EOF is also high in the MMM compared to the observation. It also explains the weaker model-simulated variability in the thermocline ridge region as observed in Section 3.2. As expected, the pattern correlation for the first EOF for all the models are above 0.7 (Figure 8). Interestingly, the correlation varies significantly for the second EOF across the models with the maximum correlation of 0.8 for CanESM5-CanOE and the negative correlation of -0.36 for the UKESM1-0-LL. Moreover, EC-Earth3 and EC-Earth3-Veg also exhibit no correlation for the second mode. In the case of explaining variance INM-CM5-0, CNRM-CM6-1-HR and HadGEM3-GC31-MM show weaker variability than observed for both the EOF modes, indicating weaker climate response in these models. In contrast, NorESM2-MM, GISS-E2-1-G and the models from the EC-Earth3 family show almost three times the observed variability for the first mode suggesting a strong bias towards the IOD mode in these models.

3.4 Skill score

Most of the models produce a very high skill score of more than 0.98 in simulating the mean DSL for the entire Indian Ocean basin (Figure 9d). In fact, the minimum score is 0.95 which is associated with the INM-CM5-0 model. The skill scores for the windstress curl don't fare as good as the sea level and lies between 0.6 and 0.8 with a few outliers (Figure 9d. Even though the models have a good spatial correlation for windstress curl, the larger and varying normalized standard deviations cause the inter-model spread in the skill scores. Note, however, that the skill score is dependent on the choice of the reference dataset as well. For example, the model windstress is more correlated to QuikSCAT scatterometer winds than the ERA-5 and produce a marginally higher skill score (Figure not shown). Nevertheless, while the choice of reference dataset yields marginally different skill scores, the outlying behaviour of most models remains the same. Since ERA-5 is available for a longer period spanning 4 decades compared to QuikSCAT observation which is only available for a decade (1999-2009), we prefer ERA-5 for further analyses in this paper. Interestingly, the skill score differs significantly across the different latitude belts. For example, the skill score in simulating DSL is in general relatively low for the NIO ranging from 0.75-0.98 with only three models could score more than 0.95. In the STIO, most models score higher in simulating sea level, suggesting that the subtropical gyre is simulated reasonably well in the Indian Ocean by most models. In the SIO, most models produce sea level reasonably well with a score of more than 0.85 except for a few outliers. Notably, here the model skill in simulating windstress curl is the maximum with a usual score of more than 0.85 despite models predominantly produce anomalously strong westerlies. This discrepancy is due to the fact that the skill score depends only on correlation and its variability and not the magnitude of the variable. Hence, while skill score can provide a picture of the overall performance of each model, but it should be considered along with other statistical/physical characteristics of model simulations as well.

3.5 Projection

Most CMIP6 models conserve volume rather than mass and therefore, any change in the temperature of the water column does not necessarily reflect in the sea level change. In order to account for this effect, we followed the method adopted in Richter et al. (2017) wherein the dynamic sea level change (*zos*) is added to the global mean thermosteric sea level change (*zostoga*) after removing the global mean of *zos* at each time step. This allows the regional dynamical change consisting of changes due to local winds, thermal expansion and the change in global mean steric height. Two models MRI-ESM2-0 and INM-CM5-0 could not be considered for the analysis due to inconsistency in *zostoga* (MRI-

ESM2-0 show discontinuity in the *zostoga* time-series and INM-CM5-0 show insistent *zostoga* compared to the rest of the model simulations (Figure S3)) and for two model future projections of DSL is not available at the time of this analysis.

Considering that a few models completely failed to simulate the historical dynamic sea level, its variability and the primary wind forcing, we have used a few subjective criteria to discard these unrealistic models to get the most appropriate estimates. We mainly considered the mean state biases and the representation of variability and climate modes to select the best-performing models. Hence, the skill score of the model simulated sea level and wind field for the entire basin is considered to identify the outliers. The minimum benchmark skill score for a model to qualify is set to 0.98 for dynamic sea level and 0.7 for the windstress curl over the entire IO. This allows only 10 models to qualify for the next screening criterion and discarded 15 models. Next, we looked at the key climate features among these 10 models to identify any unrealistic simulations. In this test, we remove three more models further and they are EC-Earth3, EC-Earth3-Veg and NorESM2-MM. This allows us to use only seven models for the best estimate of the projected dynamic sea level and wind fields. These models are BCC-ESM-MR, CNRM-CM6-1-HR, IPSL-CM6A-LR, CMCC-CM2-SR5, CMCC-CM2-HR4, EC-Earth-Veg-LR, CNRM-ESM2-1 and CNRM-CM6-1.

In order to calculate the projected changes over the Indian ocean for mid-emission (SSP2-4.5) and high-emission (SSP5-8.5) radiative forcing the averaged departure of projected variable for 2080-2100 relative to the historical period of 1994-2014 is considered. Both the scenarios show a similar projected patterns and differ primarily in magnitudes (Figure 10). Interestingly, the ensemble of the best performing model shows a weaker sea level rise in the IO compared to the full MMM solution. In NIO, the Arabian Sea shows a stronger rise in sea level compared to the Bay of Bengal. The best model estimate shows a sea level rise of ~22-25 cm under the SSP2-4.5 scenario and ~35 cm rise for the SSP5-8.5 scenario. The western Bay of Bengal also shows a similar rising trend as in the Arabian Sea, but indicate a much weaker rise of DSL in the eastern part. While this increase in sea level is primarily driven by the warming of the water column, ~12-15% is contributed by the weakening of the summer monsoon wind field. The SIO also shows a strong sea level rise along the ACC current regime. This increase in sea level is linked to the poleward shift of the Southern Ocean westerlies due to warming of the Southern Ocean driven by the anthropogenic forcing. Under the SSP5-8.5 scenario, the maximum sea level rise in this region is expected to be ~35-40 cm. In contrast, the STIO latitude band show the minimum sea level rise driven by the weakening of the trade winds.

Like the mean field, the variability of the sea level also shows a similar pattern in the projected change under the SSP2-4.5 and SSP5-8.5 scenarios. However, note that, in contrast to the mean field, the best estimate of the ensemble mean variability is generally higher in the entire basin compared to the mean field. The western Arabian sea shows the strongest increase in the sea level variability with an increase of ~30% compared to the historical period under the high emission scenario. This is a significant increase over the CMIP5 model estimates on the projected variability of this region (see Figure 8e of Deepa et al., 2021). The AICC current regime of the SIO and the west coast of Australia also show a considerable increase in the sea level variability. The thermocline ridge region, however, shows a marked decrease in variability which is in agreement with the CMIP5 models (Deepa et al., 2021). Notably, the thermocline ridge region is shown to be one of the internal variabilities dominated regions (Han et al., 2014). Therefore, considering that the CMIP6 models underestimate the variability of this region (Figure 7), the projected decreasing variability of this region should be treated cautiously. In contrast, unlike CMIP5 model, CMIP6 models project a stronger increase in sea level variability in the eastern equatorial Indian Ocean and along the coast of Java, suggesting the

influence of an increase in effective climate sensitivity of the CMIP6 models as reported earlier by Hermans et al., (2021). Further, the overestimation of the dipole strength in the CMIP6 modes is also likely to impact the long-term climate signatures of this tropical basin.

4. Conclusion

In this study, we evaluate the skill of models participating in the Sixth phase of coupled 10model intercomparison project (CMIP6) in simulating the DSL and the associated wind field over the Indian ocean. Subsequently, we select a subset of models by discarding grossly biased models from the ensemble to get the best-estimated projections over the Indian Ocean. Models' ability to reproduce the mean states, variability and climate modes for the observational period is used to assess the skills for each model. We use statistical tools such as pattern correlation, RMSE, and skill score metrics based on Taylor (2001) to assess the performance of models. Projections of sea level and wind field are analysed for moderate (SSP2-4.5) and high (SSP5-8.5) radiation forcing future scenarios.

Most models could reproduce the mean DSL of the IO very well with a skill score of more than 0.95. However, the skill score varies considerably across the latitude band with the lowest scores exhibited in the NIO. All the models show consistent biases in sea level and winds in a few dynamically dominated regions. Nevertheless, the zonally averaged DSL show consistent positive bias across all latitude with maximum bias in the ACC regime. Also, the equatorward shift of the Southern Ocean westerlies is found to be more in the Indian Ocean compared to the global averaged. In the NIO, the weaker summer monsoon winds in the model cause weak coastal upwelling along the western boundary of the Arabian Sea, resulting in a positive bias in the western IO.

The equatorward shift of the southwesterly trade winds causes anomalous easterly winds along the equator in most models. These wind biases soals the thermocline of the eastern equatorial IO and reduce the west-east sea level (thermocline) tilt which is otherwise found in the observations. This relatively flat equatorial thermocline enhances the air-sea feedback and causes a dipole pattern in SST and sea level in the tropical basin. This IOD like bias is also reflected in the EOF analysis with stronger than observed variability in the first EOF mode. Some of the models such as NorESM2-MM, GISS-E2-1-G and the models from the EC-Earth3 family exhibits almost three times of the observed variability indicating a strong bias towards the IOD mode.

In the case of variability, model simulations in general underestimate from the observation across the entire basin except for the eastern equatorial IO and the Sumatran coast. The overestimated magnitude of variability along the Sumatran coast is likely due to the shallow mixed layer driven by the easterly bias in the equatorial zonal winds. As expected, the high-resolution models reproduce the observed variability better compared to the coarser models, particularly in the high eddy dominated regions like ACC current regime.

The sea-level change towards the end of the century is calculated as the difference between the sea level averaged over the last two decades of the projection (2080-2100) and historical simulations (1994-2014). Both scenarios show a similar spatial pattern of sea-level change with differences in magnitude. The spatial pattern of the sea level change shows a west-to-east gradient in the northern IO with a significant rise in the Arabian Sea and along the east coast of India. This projected sea level rise in the Arabian Sea is primarily due to the warming of the water column and weakened summer monsoon winds. The STIO, in contrast, shows an overall dip in the projected sea level. In terms of variability, the western Arabian Sea show a 30% increase in projected sea level variability. In the SIO,

the ACC current regime also shows a marked projected increase but shifted poleward as the westerly winds are also projected to move poleward owing to the anthropogenic warming of the Southern Ocean.

Finally, the best estimate of sea level projection based on an ensemble of seven best performing climate models indicates a slightly weaker rise in projected sea level compared to MMM ensemble but show higher projected variability in the entire basin.

Acknowledgements

We acknowledge the financial support provided by Indian National Centre for Ocean Information Services (INCOIS), Ministry of Earth Sciences(MoES), Govt. of India, to conduct this research. The first author is grateful to CSIR, India for the Ph D fellowship, Kerala University of Fisheries and Ocean Studies(KUFOS) for providing the necessary facilities. This is INCOIS contribution number XXXX.

Table

No	Source id	Grid info	Historical simulation	Projected simulations
1	ACCESS-CM2	360 x 300	✓	
2	ACCESS-ESM1-5	360 x 300	✓	
3	BCC-CSM2-MR	360 x 232	✓	✓
4	BCC-ESM1	360 x 232	✓	
5	CMCC-CM2-HR4	1051 x 1442	✓	✓
6	CMCC-CM2-SR5	292 x 362	✓	✓
7	CNRM-CM6-1	362 x 294	✓	✓
8	CNRM-CM6-1-HR	1442 x 1050	✓	✓
9	CNRM-ESM2-1	362 x 294	✓	✓
10	CanESM5	360 x 291	✓	
11	CanESM5-CanOE	360 x 291	✓	
12	EC-Earth3	362 x 292	✓	
13	EC-Earth3-Veg	362 x 292	✓	
14	EC-Earth3-Veg-LR	362 x 292	✓	✓
15	GISS-E2-1-G	288 x 180	✓	
16	HadGEM3-GC31-LL	360 x 330	✓	
17	HadGEM3-GC31-MM	1440 x 1205	✓	
18	INM-CM5-0	360 x 180	✓	
19	IPSL-CM6A-LR	362 x 332	✓	✓
20	MIROC6	360 x 256	✓	
21	MPI-ESM-1-2-HAM	256 x 220	✓	
22	MPI-ESM1-2-HR	802 x 404	✓	
23	MPI-ESM1-2-LR	256 x 220	✓	

24	MRI-ESM2-0	360 x 363	✓	
25	NorESM2-LM	360 x 385	✓	
26	NorESM2-MM	360 x 385	✓	
27	UKESM1-0-LL	360 x 330	✓	

Table 1: List of 27 CMIP6 models used in this study. The models used for historical simulation assessment and the models sected for best estimate of projection are identified using check boxes.

Figures

Figure 1: Comparison of mean dynamic sea level (top) and windstress curl (bottom; shaded) overlayed by the mean winds (vectors) from observation (left), MMM (middle) and bias (right).

Figure 2: Zonally averaged dynamic sea level (left), zonal windstress (middle) and windstress curl (right) from observation (dotted black) and model. The shaded area represents model spread.

Figure 3: Top panels show spread of the model simulated sea level bias for NIO (left), STIO (middle) and SIO (right). Bottom panels show RMSE for individual models for each latitude bands.

Figure 4: Sea level variability for the period 1993-2014 from (a) altimeter observation (b) multi-model mean and (c) model bias. Panels (d,e,f) and (g,h,i) are for the annual and interannual signals, respectively.

Figure 5: Pattern correlation and RMSE of sea level variability for (a,b) total, (c,d) annual and (e,f) interannual signals. The whiskers represents the spread of corresponding metric across the 20-year sliding window.

Figure 6: (a) The equatorial mean dynamic state of sea level averaged over 2^{o}N-2^{o}S from observation (dashed black), multi-model mean (dashed blue) and all the CMIP6 models (solid thin blue). (b) Same as (a) but for zonal windstress. (c) pattern correlation equatorial multi-model mean dynamic sea level relative to the altimeter observations (blue bars) and the corresponding RMSE (green squares). (d) Same as (c) but for zonal windstress.

Figure 7: Comparison of the first (top) and second (bottom) EOF modes of detrended interannual dynamic sea level from observation (left) and multi-model mean (right).

Figure 8: Pattern correlation and variability for the first and second EOF modes of the detrended interannual dynamic sea level from CMIP6 models relative to the altimeter observations.

Figure 9: Scatter diagram of the skill score for the model simulated sea level and windstress curl for the NIO (top left), STIO (top right), SIO (bottom left) and the entire Indian Ocean (bottom right).

Figure 10: Projected change in the mean dynamic sea level (top), magnitude of the windstress with windstress vectors overlayed (centre) and windstress curl (right) for all models (top) and selected models (upper middle) for the SSP2-4.5 scenario and for all models (lower middle) and selected models (bottom) for the SSP5-8.5 scenarios.

Figure 11: Same as Figure 10, but for the standard deviations.

Supplementry Figures

Figure S1: Model simulated mean windstress curl (shaded) overlayed by the mean winds (vectors) for all CMIP6 models.

Figure S2: Total standard deviation (cm) of individual CMIP6 models.

Figure S3: Timeseries of zostoga from all the CMIP6 models.

References

Andrews, T., Gregory, J. M., Webb, M. J., and Taylor, K. E. (2012). Forcing, feedbacks and climate sensitivity in CMIP5 coupled atmosphere-ocean climate models. Geophysical Research Letters, 39, 1– 7. https://doi.org/10.1029/2012GL051607

Beal, L.M. and Donohue, K.A. (2013). The Great Whirl: Observations of its seasonal development and interannual variability. Journal of Geophysical Research: Oceans, 118(1), pp.1-13.

Bindoff, N. L., J. Willebrand, V. Artale, A. Cazenave, J. M. Gregory, S. Gulev, K. Hanawa, C. Le Quere, S. Levitus, Y. Nojiri, et al. (2007) Observations: oceanic climate change and sea level. In: Climate Change 2007: The Physical Science Basis. Contribution of Working Group I to the Fourth Assessment Report of the Intergovernmental Panel on Climate Change [Solomon, S., D. Qin, M. Manning, Z. Chen, M. Marquis, K.B. Averyt, M. Tignor and H.L. Miller (eds.)]. Cambridge University Press, Cambridge, United Kingdom and New York, NY, USA. http://nora.nerc.ac.uk/id/eprint/15400.

Brunner, L., Pendergrass, A. G., Lehner, F., Merrifield, A. L., Lorenz, R., & Knutti, R. (2020). Reduced global warming from CMIP6 projections when weighting models by performance and independence. Earth System Dynamics, 11, 995– 1012. https://doi.org/10.5194/esd-11-995-2020.

Cai, W. and Cowan, T. (2013) Why is the amplitude of the Indian Ocean dipole overly large in CMIP3 and CMIP5 climate models?. Geophysical Research Letters, 40(6), pp.1200-1205.

Cazenave, A. and Cozannet, G.L. (2014). Sea level rise and its coastal impacts. Earth's Future, 2(2), pp.15-34.

Chatterjee, A., Kumar, B.P., Prakash, S. and Singh, P. (2019). Annihilation of the Somali upwelling system during summer monsoon. Scientific reports, 9(1), pp.1-14.

Chatterjee, A., Shankar, D., McCreary, J.P., Vinayachandran, P.N. and Mukherjee, A. (2017). Dynamics of Andaman Sea circulation and its role in connecting the equatorial Indian Ocean to the Bay of Bengal. Journal of Geophysical Research: Oceans, 122(4), pp.3200-3218.

Chatterjee, A., Shankar, D., Shenoi, S.S.C., Reddy, G.V., Michael, G.S., Ravichandran, M., Gopalkrishna, V.V., Rao, E.R., Bhaskar, T.U. and Sanjeevan, V.N., 2012. A new atlas of temperature and salinity for the North Indian Ocean. Journal of Earth System Science, 121(3), pp.559-593.

Christensen, J.H. and Christensen, O.B., 2007. A summary of the PRUDENCE model projections of changes in European climate by the end of this century. Climatic change, 81(1), pp.7-30.

Church, J.A., Clark, P.U., Cazenave, A., Gregory, J.M., Jevrejeva, S., Levermann, A., Merrifield, M.A., Milne, G.A., Nerem, R.S., Nunn, P.D. and Payne, A.J., (2013). Sea level change. PM Cambridge University Press.

Church, J.A. and White, N.J., (2011). Sea-level rise from the late 19th to the early 21st century. Surveys in geophysics, 32(4), pp.585-602.

Deepa, J. S., C. Gnanaseelan, and A. Parekh. “The sea level variability and its projections over the Indo-Pacific Ocean in CMIP5 models.” Climate Dynamics 57, no. 1 (July 2021): 173–193. doi:10.1007/s00382-021-05701-3.

Eyring, V., Bony, S., Meehl, G.A., Senior, C.A., Stevens, B., Stouffer, R.J. and Taylor, K.E., 2016. Overview of the Coupled Model Intercomparison Project Phase 6 (CMIP6) experimental design and organization. Geoscientific Model Development, 9(5), pp.1937-1958.

Fathrio, I., Iizuka, S., Manda, A., Kodama, Y.M., Ishida, S., Moteki, Q., Yamada, H. and Tachibana, Y., 2017. Assessment of western I ndian O cean SST bias of CMIP5 models. Journal of Geophysical Research: Oceans, 122(4), pp.3123-3140.

Fyfe, J. C., and O. A. Saenko, 2006: Simulated changes in the extratropical Southern Hemisphere winds and currents. Geophys.Res. Lett., 33, L06701, https://doi.org/10.1029/2005GL025332.

Greene, A.M., Goddard, L. and Lall, U., 2006. Probabilistic multimodel regional temperature change projections. Journal of Climate, 19(17), pp.4326-4343.

Gregory, J. M.,and Coauthors, 2019: Concepts and terminology for sea level:Mean, variability and change, both local and global. Surv. Geophys.,40, 1251–1289, https://doi.org/10.1007/s10712-019-09525-z.

Griffies, S.M., Danabasoglu, G., Durack, P.J., Adcroft, A.J., Balaji, V., Böning, C.W., Chassignet, E.P., Curchitser, E., Deshayes, J., Drange, H. and Fox-Kemper, B., (2016). OMIP contribution to CMIP6: Experimental and diagnostic protocol for the physical component of the Ocean Model Intercomparison Project. Geoscientific Model Development, 9(9), pp.3231-3296.

Halder, S., Parekh, A., Chowdary, J.S., Gnanaseelan, C. and Kulkarni, A., (2021) Assessment of CMIP6 models' skill for tropical Indian Ocean sea surface temperature variability. International Journal of Climatology, 41(4), pp.2568-2588.

Ham, Y. G., and J. S. Kug (2015) Improvement of ENSO simulation based on intermodel diversity. J. Climate, 28, 998–1015, https://doi.org/10.1175/JCLI-D-14-00376.1.

Han, W., G. A. Meehl, B. Rajagopalan, J. T. Fasullo, A. Hu, J. Lin, W. G. Large, et al. (2010) Patterns of Indian Ocean sea-level change in a warming climate. Nature Geoscience, 3, 546–550. doi:10.1038/ngeo901.

Han, W., Vialard, J., McPhaden, M.J., Lee, T., Masumoto, Y., Feng, M. and De Ruijter, W.P., 2014. Indian Ocean decadal variability: A review. Bulletin of the American Meteorological Society, 95(11), pp.1679-1703.

Hermans, T.H., Gregory, J.M., Palmer, M.D., Ringer, M.A., Katsman, C.A. and Slangen, A.B., (2021). Projecting global mean sea-level change using CMIP6 models. Geophysical Research Letters, 48(5), p.e2020GL092064.

IPCC, 2021: Climate Change 2021: The Physical Science Basis. Contribution of Working Group I to the Sixth Assessment Report of the Intergovernmental Panel on Climate Change [Masson-Delmotte, V., P. Zhai, A. Pirani, S.L. Connors, C. Péan, S. Berger, N. Caud, Y. Chen, L. Goldfarb, M.I. Gomis, M. Huang, K. Leitzell, E. Lonnoy, J.B.R. Matthews, T.K. Maycock, T. Waterfield, O. Yelekçi, R. Yu, and B. Zhou (eds.)]. Cambridge University Press. In Press.

Jia, F., Wu, L., Lan, J. and Qiu, B. (2011). Interannual modulation of eddy kinetic energy in the southeast Indian Ocean by Southern Annular Mode. Journal of Geophysical Research: Oceans, 116(C2).

Kim, Y.S. and Orsi, A.H., 2014. On the variability of Antarctic Circumpolar Current fronts inferred from 1992–2011 altimetry. Journal of Physical Oceanography, 44(12), pp.3054-3071.

Krishnan, A. and Bhaskaran, P.K., 2019. CMIP5 wind speed comparison between satellite altimeter and reanalysis products for the Bay of Bengal. Environmental monitoring and assessment, 191(9), pp.1-17.

Lakshmi, R.S., Chatterjee, A., Prakash, S. and Mathew, T., 2020. Biophysical interactions in driving the summer monsoon chlorophyll bloom off the Somalia coast. Journal of Geophysical Research: Oceans, 125(3), p.e2019JC015549.

Landerer FW, Jungclaus JH, Marotzke J (2007) Regional dynamic and steric sea level change in response to the IPCC-A1B scenario. J Phys Oceanogr 37(2):296. doi:10.1175/JPO3013.1

Landerer, F.W., Gleckler, P.J. and Lee, T. (2014). Evaluation of CMIP5 dynamic sea surface height multi-model simulations against satellite observations. *Climate dynamics*, *43*(5-6), pp.1271-1283.

Lowe, J.A. and Gregory, J.M. (2006). Understanding projections of sea level rise in a Hadley Centre coupled climate model. Journal of Geophysical Research: Oceans, 111, C1104. doi:10.1029/2005JC003421.

Lyu, K., Zhang, X. and Church, J.A. (2020a). Regional dynamic sea level simulated in the CMIP5 and CMIP6 models: mean biases, future projections, and their linkages. Journal of Climate, 33(15), pp.6377-6398.

Lyu, K., Zhang, X., Church, J.A. and Wu, Q. (2020b) Processes responsible for the Southern Hemisphere ocean heat uptake and redistribution under anthropogenic warming. Journal of Climate, 33(9), pp.3787-3807.

Maximenko, N., Niiler, P., Centurioni, L., Rio, M.H., Melnichenko, O., Chambers, D., Zlotnicki, V. and Galperin, B., 2009. Mean dynamic topography of the ocean derived from satellite and drifting buoy data using three different techniques. Journal of Atmospheric and Oceanic Technology, 26(9), pp.1910-1919.

McGregor S, Gupta AS, England MH (2012) Constraining wind stress products with sea surface height observations and implications for Pacific Ocean sea level trend attribution. J Clim 25(23):8164. doi:10.1175/JCLI-D-12-00105.1

McSweeney, C.F., Jones, R.G., Lee, R.W. and Rowell, D.P., 2015. Selecting CMIP5 GCMs for downscaling over multiple regions. Climate Dynamics, 44(11), pp.3237-3260.

Meehl, G.A., Covey, C., Delworth, T., Latif, M., McAvaney, B., Mitchell, J.F., Stouffer, R.J. and Taylor, K.E. (2007). The WCRP CMIP3 multimodel dataset: A new era in climate change research. Bulletin of the American meteorological society, 88(9), pp.1383-1394.

Menezes, V. V., H. E. Phillips, A. Schiller, N. L. Bindoff, C. M. Domingues, and M. L. Vianna (2014b), South Indian Countercurrent and associated fronts, J. Geophys. Res. Oceans, 119, 6763–6791, doi:10.1002/2014JC010076.

Meyssignac, B., and A. Cazenave. (2012) Sea level: A review of present-day and recent- past changes and variability. Journal of Geodynamics, 58, 96–109. doi: 10.1016/j.jog.2012.03.005.

Milne, G.A., Gehrels, W.R., Hughes, C.W. and Tamisiea, M.E. (2009). Identifying the causes of sea-level change. Nature Geoscience, 2(7), pp.471-478.

Mukherjee, A., Shankar, D., Chatterjee, A. and Vinayachandran, P.N., 2018. Numerical simulation of the observed near-surface East India Coastal Current on the continental slope. Climate Dynamics, 50(11), pp.3949-3980.

Nijsse, F. J. M. M., Cox, P. M., & Williamson, M. S. (2020). Emergent constraints on transient climate response (TCR) and equilibrium climate sensitivity (ECS) from historical warming in CMIP5 and CMIP6 models. Earth System Dynamics, 11, 737– 750. https://doi.org/10.5194/esd-11-737-2020.

O'Neill, B. C., Kriegler, E., Riahi, K., Ebi, K. L., Hallegatte, S., Carter, T. R., et al. (2014). A new scenario framework for climate change research: the concept of shared socioeconomic pathways. Climatic Change, 122, 387– 400. https://doi.org/10.1007/s10584-013-0905-2.

Oppenheimer, M., Glavovic, B., Hinkel, J., van de Wal, R., Magnan, A.K., Abd-Elgawad, A., Cai, R., Cifuentes-Jara, M., Deconto, R.M., Ghosh, T. and Hay, J. (2019) Sea level rise and implications for low lying islands, coasts and communities. In H.-O. Pörtner, et al. (Eds.), IPCC special report on the ocean and cryosphere in a
changing climate.

Perrette, M., Landerer, F., Riva, R., Frieler, K. and Meinshausen, M. (2013) A scaling approach to project regional sea level rise and its uncertainties. Earth System Dynamics, 4(1), pp.11-29.

Phillips, H. E., Tandon, A. et al. (2021) Progress in understanding of Indian Ocean circulation, variability, air–sea exchange, and impacts on biogeochemistry, Ocean Sci., 17, 1677-1751. https://doi.org/10.5194/os-17-1677-2021.

Riahi, K., D. P. van Vuuren, E. Kriegler, J. Edmonds, B. C. O'Neill, S. Fujimori, N. Bauer, et al. "The Shared Socioeconomic Pathways and their energy, land use, and greenhouse gas emissions

implications: An overview." *Global Environmental Change* 42 (2017): 153–168. doi:10.1016/j.gloenvcha.2016.05.009.

Richter, K., Øie Nilsen, J.E., Raj, R.P., Bethke, I., Johannessen, J.A., Slangen, A.B. and Marzeion, B., 2017. Northern North Atlantic Sea level in CMIP5 climate models: evaluation of mean state, variability, and trends against altimetric observations. *Journal of Climate*, *30*(23), pp.9383-9398.

Russell, J. L., K. W. Dixon, A. Gnanadesikan, R. J. Stouffer, and J. R. Toggweiler, 2006: The Southern Hemisphere westerlies in a warming world: Propping open the door to the deep ocean. J. Climate, 19, 6382–6390, https://doi.org/10.1175/JCLI3984.1.

Schott, F.A., Xie, S.P. and McCreary Jr, J.P. (2009). Indian Ocean circulation and climate variability. Reviews of Geophysics, 47(1).

Stammer, D., A. Cazenave, R. M. Ponte, and M. E. Tamisiea (2013) Causes for contem- porary regional sea level changes." Annual review of marine science, 5, 21–46. doi:10.1146/annurev-marine-121211-172406.

Suresh, I., Vialard, J., Lengaigne, M., Han, W., McCreary, J., Durand, F. and Muraleedharan, P.M. (2013). Origins of wind-driven intraseasonal sea level variations in the North Indian Ocean coastal waveguide. Geophysical Research Letters, 40(21), pp.5740-5744.

Tokarska, K. B., Stolpe, M. B., Sippel, S., Fischer, E. M., Smith, C. J., Lehner, F., & Knutti, R. (2020). Past warming trend constrains future warming in CMIP6 models. Science Advances, 6, 1– 14. https://doi.org/10.1126/sciadv.aaz9549

Unnikrishnan, A., and D. Shankar (2007). Are sea-level-rise trends along the coasts of the north Indian Ocean consistent with global estimates? Global and Planetary Change 57, 3, 301–307. doi:10.1016/j.gloplacha.2006.11.029.

Van Vuuren, D.P., Edmonds, J., Kainuma, M., Riahi, K., Thomson, A., Hibbard, K., Hurtt, G.C., Kram, T., Krey, V., Lamarque, J.F. and Masui, T., 2011. The representative concentration pathways: an overview. Climatic change, 109(1), pp.5-31.

Vialard, J., Shenoi, S.S.C., Mccreary, J.P., Shankar, D., Durand, F., Fernando, V. and Shetye, S.R., 2009. Intraseasonal response of the northern Indian Ocean coastal waveguide to the Madden-Julian Oscillation. Geophysical Research Letters, 36(14).

Vinayachandran, P.N.M., Masumoto, Y., Roberts, M.J., Huggett, J.A., Halo, I., Chatterjee, A., Amol, P., Gupta, G.V., Singh, A., Mukherjee, A., Prakash, S., Beckley, L. E., Raes, E. J. and Hood, R. (2021) Reviews and syntheses: Physical and biogeochemical processes associated with upwelling in the Indian Ocean. Biogeosciences, 18(22), pp.5967-6029.

Wang, X., Cheng, X., Liu, X., and Chen, D. (2021). Dynamics of eddy generation in the southeast tropical Indian Ocean. Journal of Geophysical Research: Oceans, 126, e2020JC016858. https:// doi.org/10.1029/2020JC016858.

Watterson IG, Whetton PH (2011) Distributions of decadal means of temperature and precipitation change under global warming. J Geophys Res Atmos 116:13

Yin J (2012) Century to multi-century sea level rise projections from CMIP5 models. Geophys Res Lett, 39(17). doi:10.1029/ 2012GL052947.

Yin J, Griffies SM, and Stouffer RJ (2010) Spatial variability of sea level rise in twenty-first century projections. J Clim, 23(17):4585. doi:10.1175/2010JCLI3533.1.

Zhang, N., Liu, G., Liu, Q., Zheng, S., and Perrie, W. (2020). Spatiotemporal variations of mesoscale eddies in the Southeast Indian Ocean. Journal of Geophysical Research: Oceans, 125, e2019JC015712. https://doi.org/10.1029/2019JC015712.

Data availability

All the datasets used in this study is available in public domain. The CMIP6 model simulation outputs are downloaded from https://esgf-node.llnl.gov/projects/esgf-llnl/. The windfiled from ECMWF Ranalysis 5th generation (ERA5) is available at https://doi.org/10.24381/cds.f17050d7. The gridded altimeter data is obtained from Copernicus Marine Service data respiratory https://resources.marine.copernicus.eu/.

Funding

Author SCK received a research fellowship supported by the Council of Scientific and Industrial Research (CSIR), India towards his PhD programme. AC is supported by funding from the Indian National Centre for Ocean Information Services (INCOIS), India.

Competing Interests

The authors have no relevant financial or non-financial interests to declare.

Author contributions

All authors contributed to the conceptualization and design of the study. Data download, ploting was done by SCK. All authors analysed the data, discussed the results and wrote the paper. All authors read and approved the final submitted manuscript.

Figures

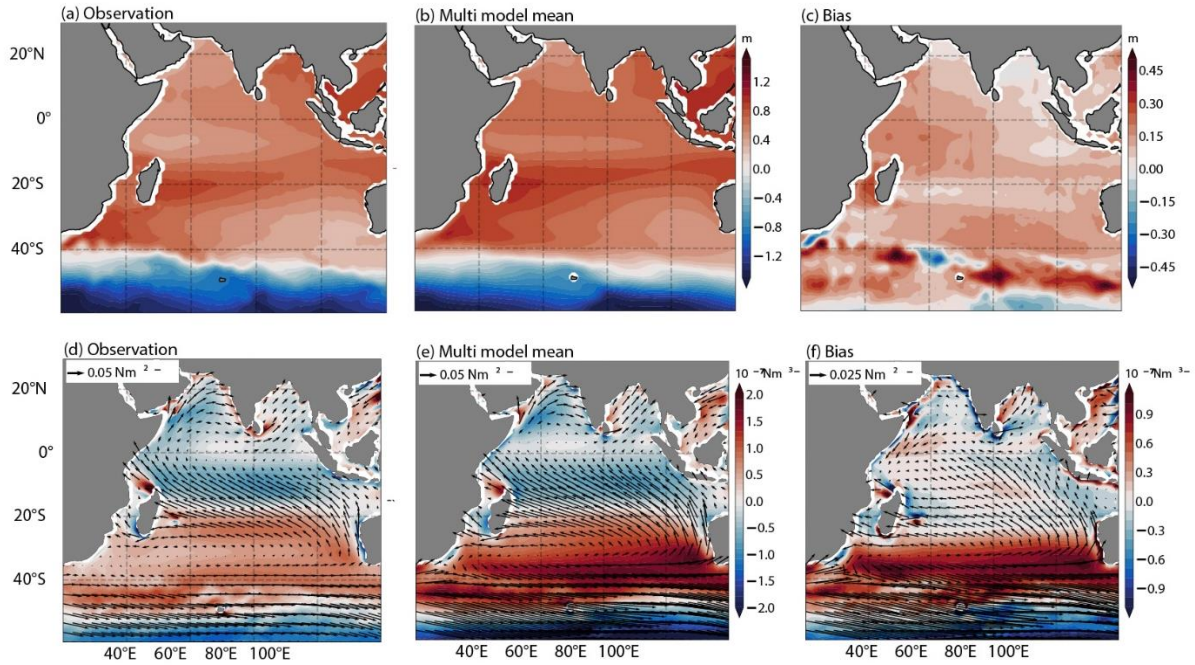

Figure 1: Comparison of mean dynamic sea level (top) and windstress curl (bottom; shaded) overlayed by the mean winds (vectors) from observation (left), MMM (middle) and bias (right).

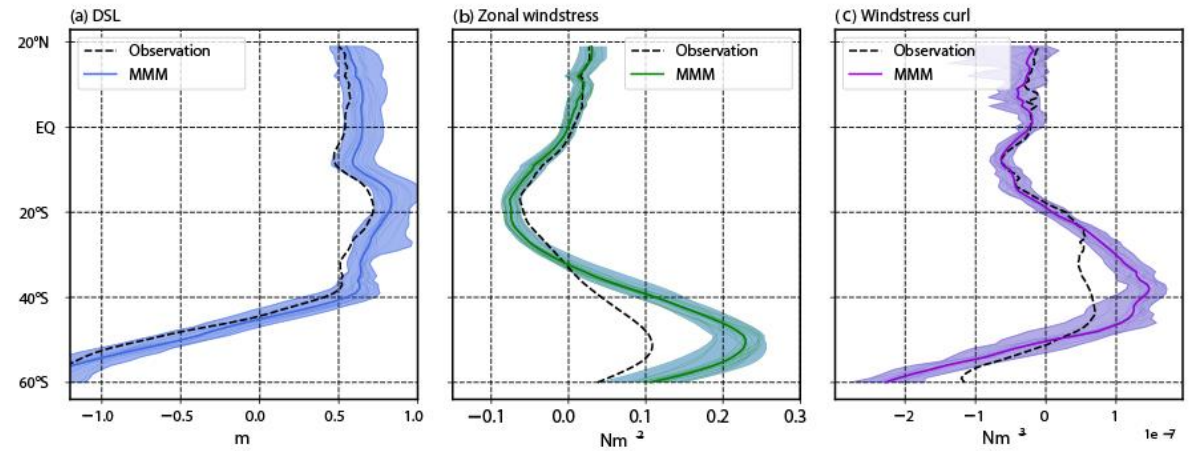

Figure 2: Zonally averaged dynamic sea level (left), zonal windstress (middle) and windstress curl (right) from observation (dotted black) and model. The shaded area represents model spread.

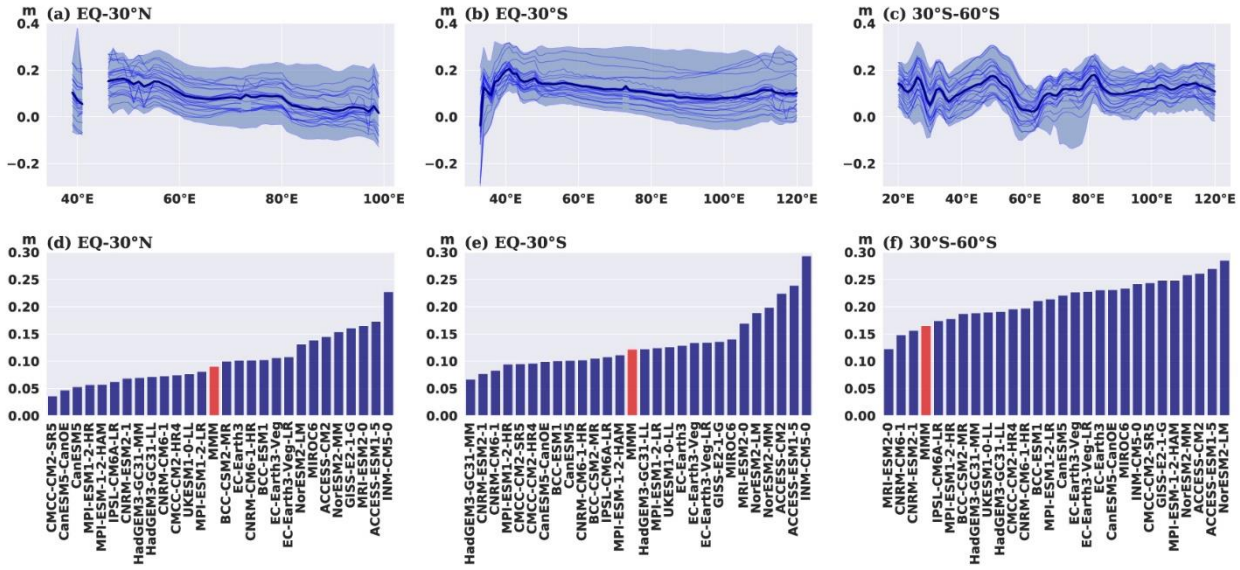

Figure 3: Top panels show spread of the model simulated sea level bias for NIO (left), STIO (middle) and SIO (right). Bottom panels show RMSE for individual models for each latitude bands.

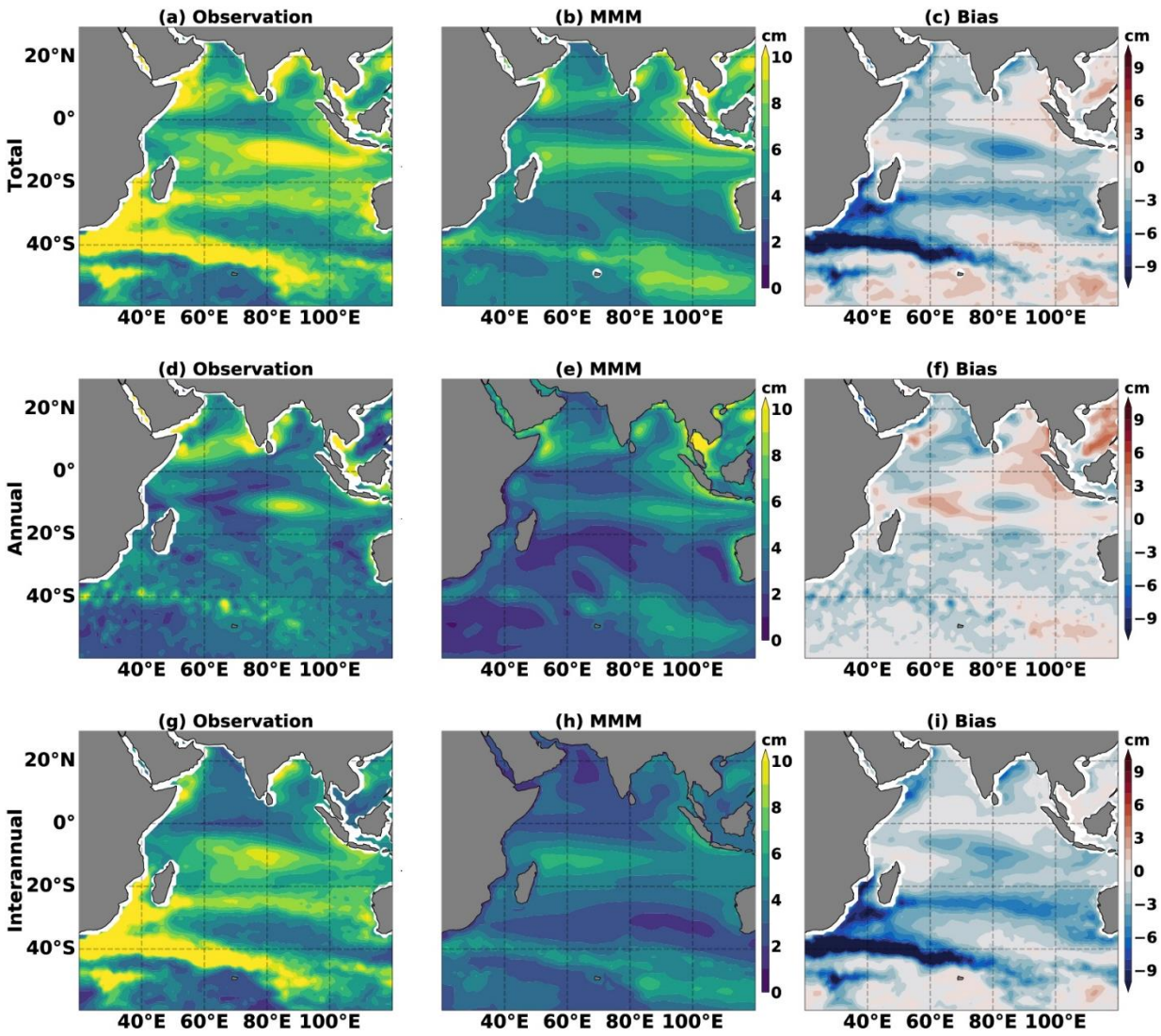

Figure 4: Sea level variability for the period 1993-2014 from (a) altimeter observation (b) multi-model mean and (c) model bias. Panels (d,e,f) and (g,h,i) are for the annual and interannual signals, respectively.

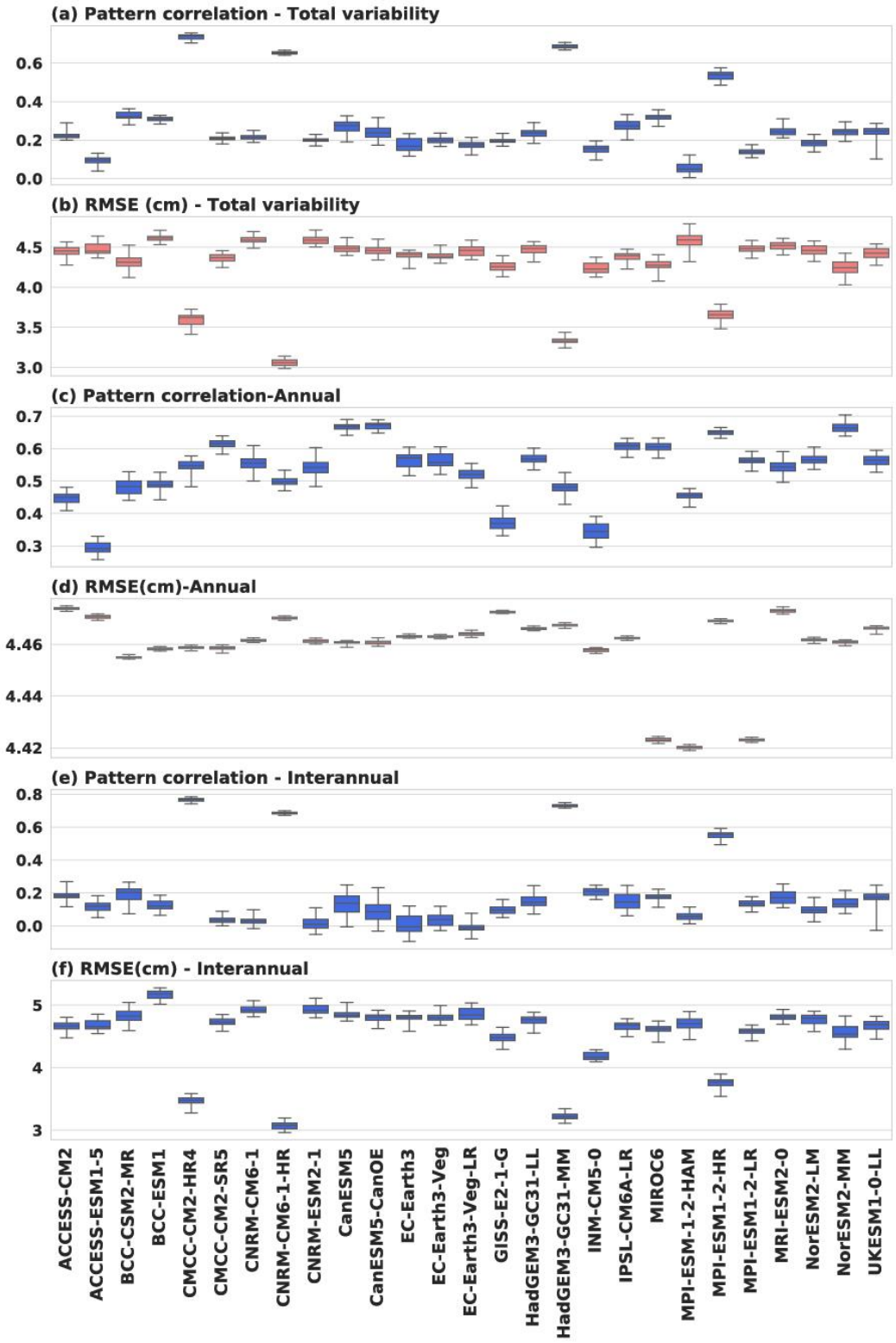

Figure 5: Pattern correlation and RMSE of sea level variability for (a,b) total, (c,d) annual and (e,f) interannual signals. The whiskers represents the spread of corresponding metric across the 20-year sliding window.

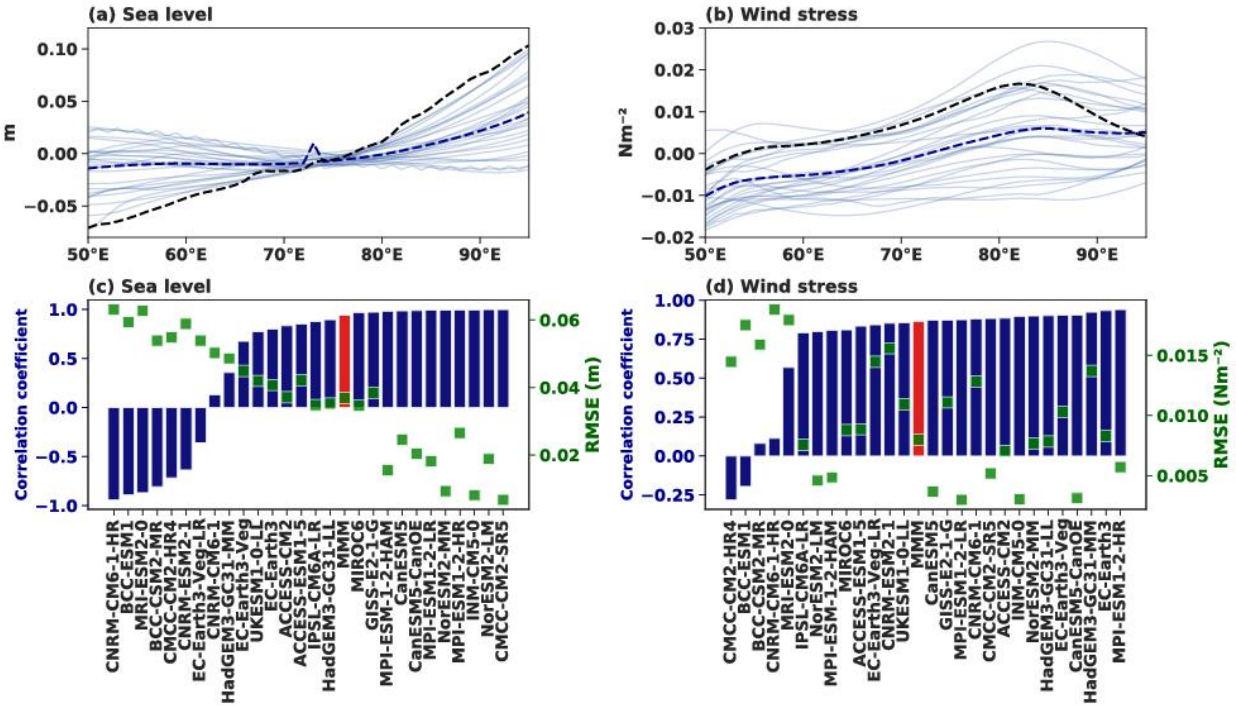

Figure 6: (a) The equatorial mean dynamic state of sea level averaged over 2°N-2°S from observation (dashed black), multi-model mean (dashed blue) and all the CMIP6 models (solid thin blue). (b) Same as (a) but for zonal windstress. (c) pattern correlation equatorial multi-model mean dynamic sea level relative to the altimeter observations (blue bars) and the corresponding RMSE (green squares). (d) Same as (c) but for zonal windstress.

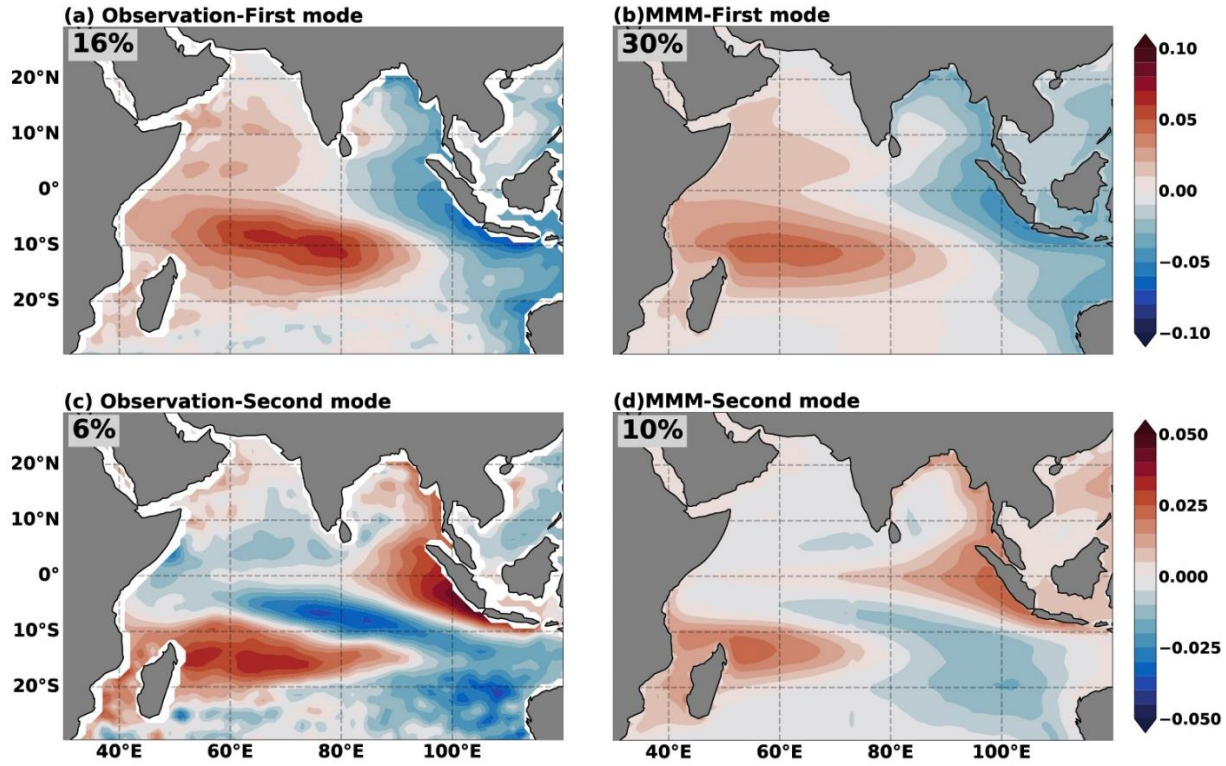

Figure 7: Comparison of the first (top) and second (bottom) EOF modes of detrended interannual dynamic sea level from observation (left) and multi-model mean (right).

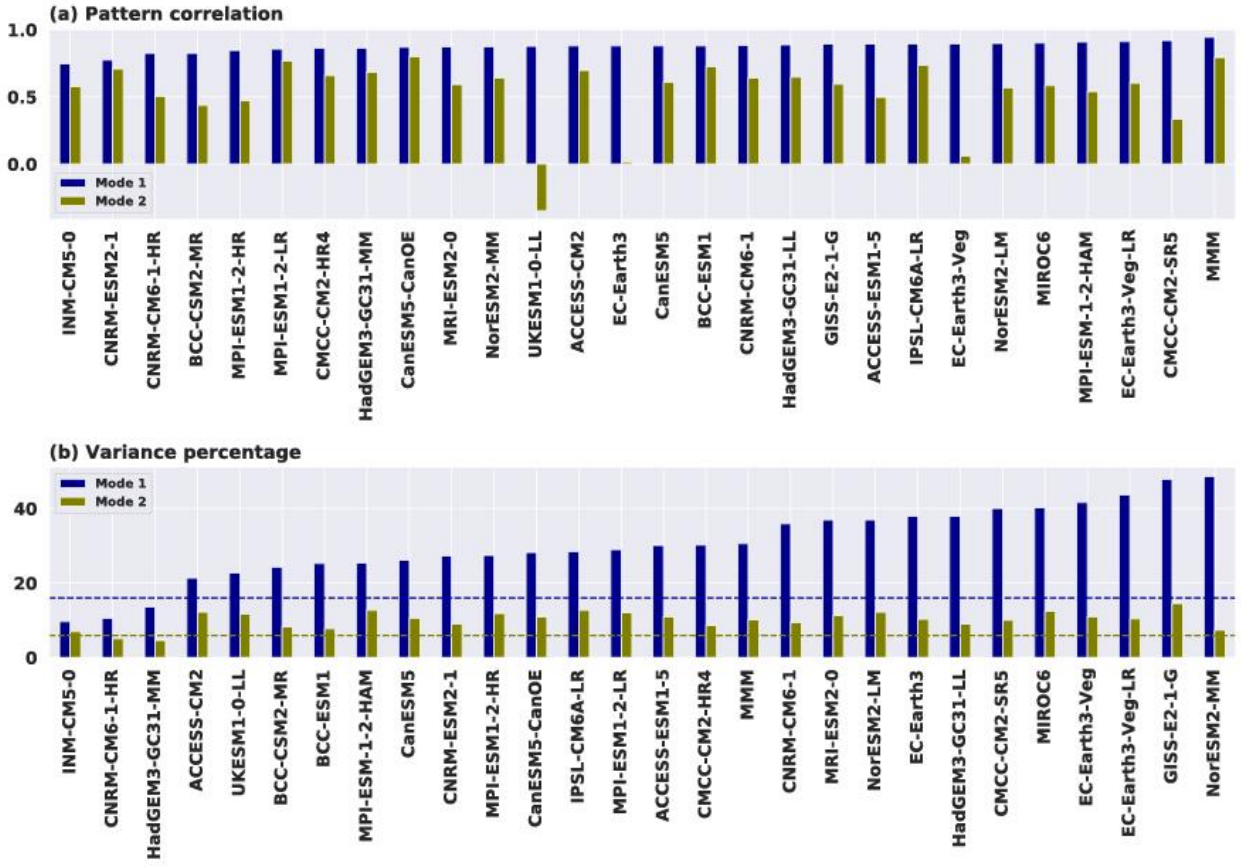

Figure 8: Pattern correlation and variability for the first and second EOF modes of the detrended interannual dynamic sea level from CMIP6 models relative to the altimeter observations.

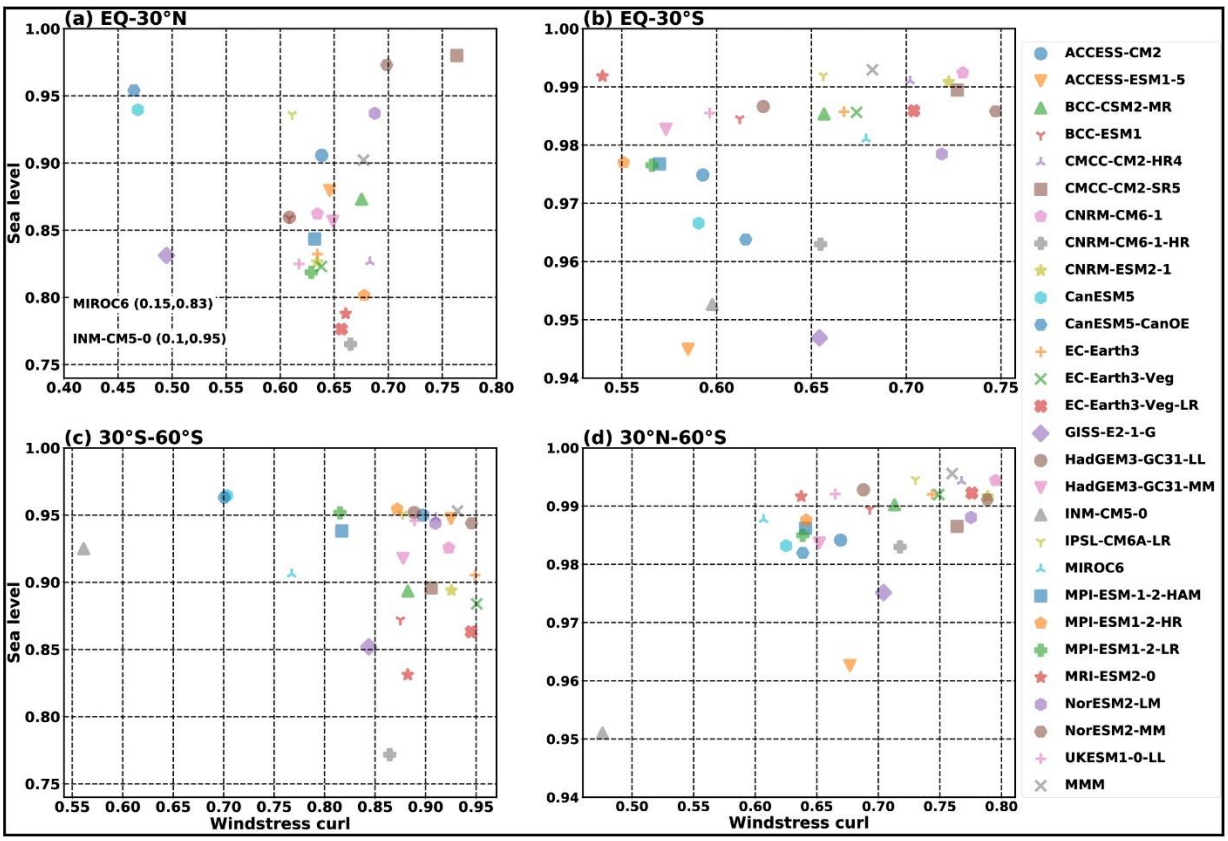

Figure 9: Scatter diagram of the skill score for the model simulated sea level and windstress curl for the NIO (top left), STIO (top right), SIO (bottom left) and the entire Indian Ocean (bottom right).

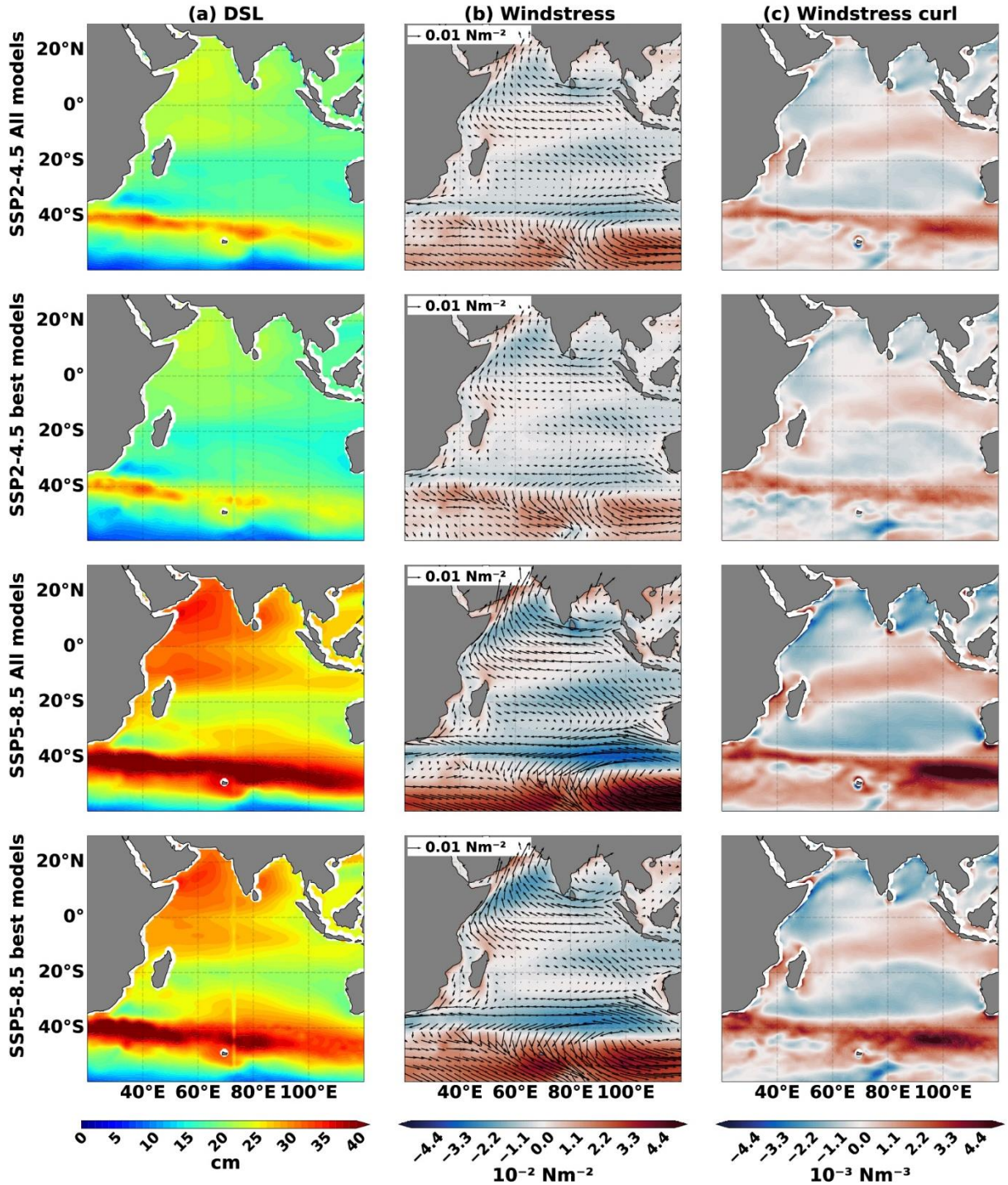

Figure 10: Projected change in the mean dynamic sea level (top), magnitude of the windstress with windstress vectors overlayed (centre) and windstress curl (right) for all models (top) and selected models (upper middle) for the SSP2-4.5 scenario and for all models (lower middle) and selected models (bottom) for the SSP5-8.5 scenarios.

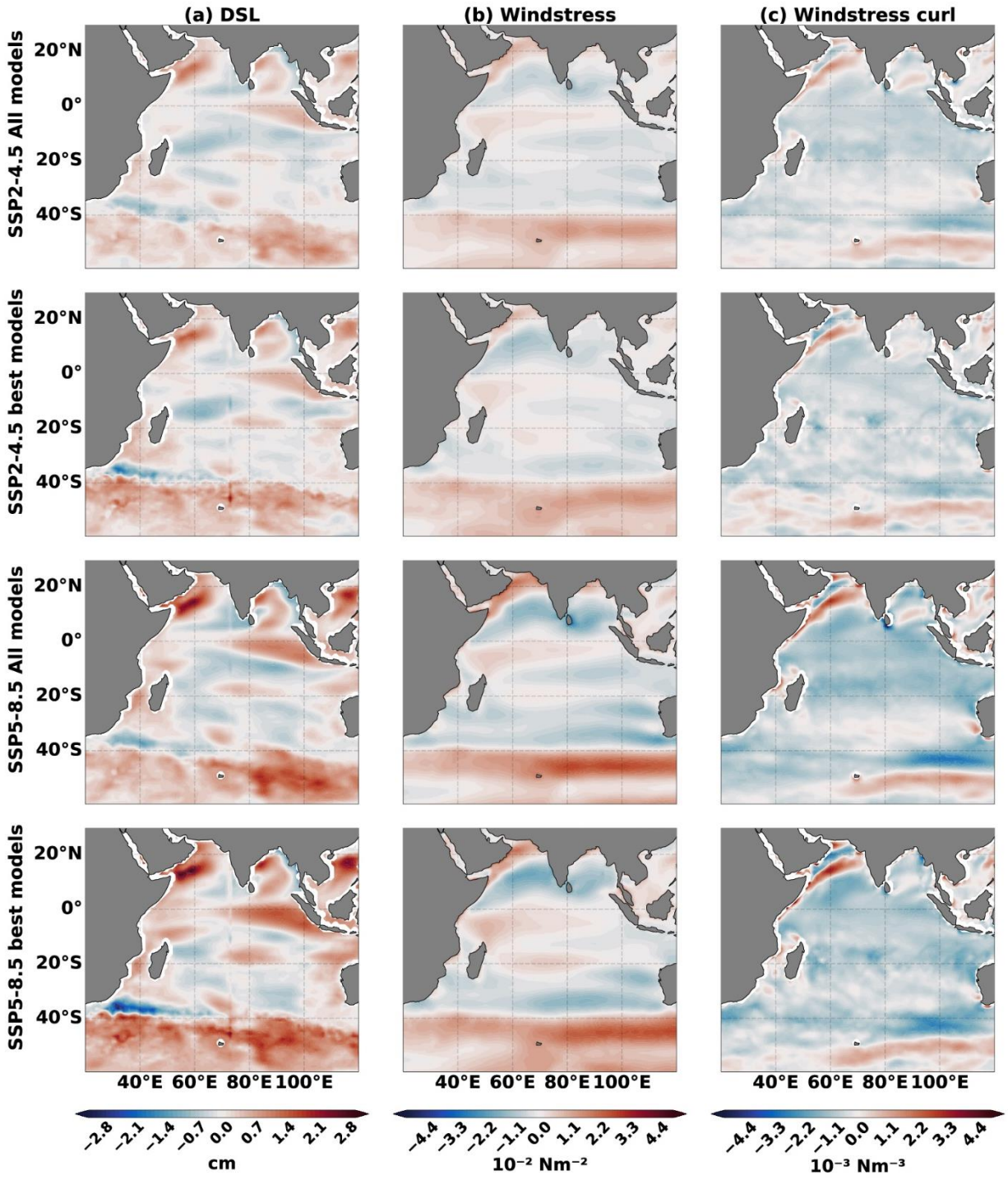

Figure 11: Same as Figure 10, but for the standard deviations.

Supplementary figures

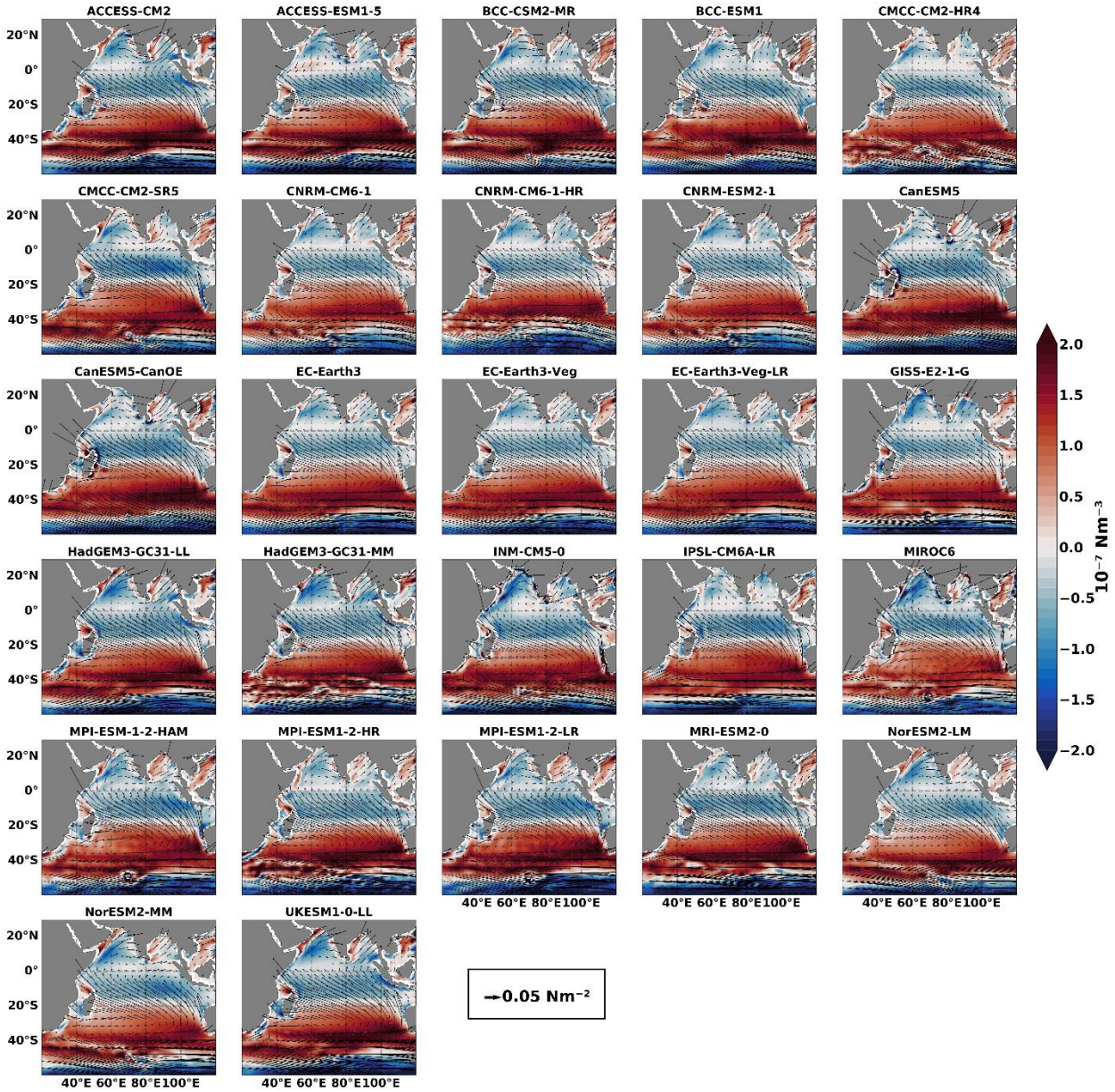

Figure S1: Model simulated mean windstress curl (shaded) overlayed by the mean winds (vectors) for all CMIP6 models.

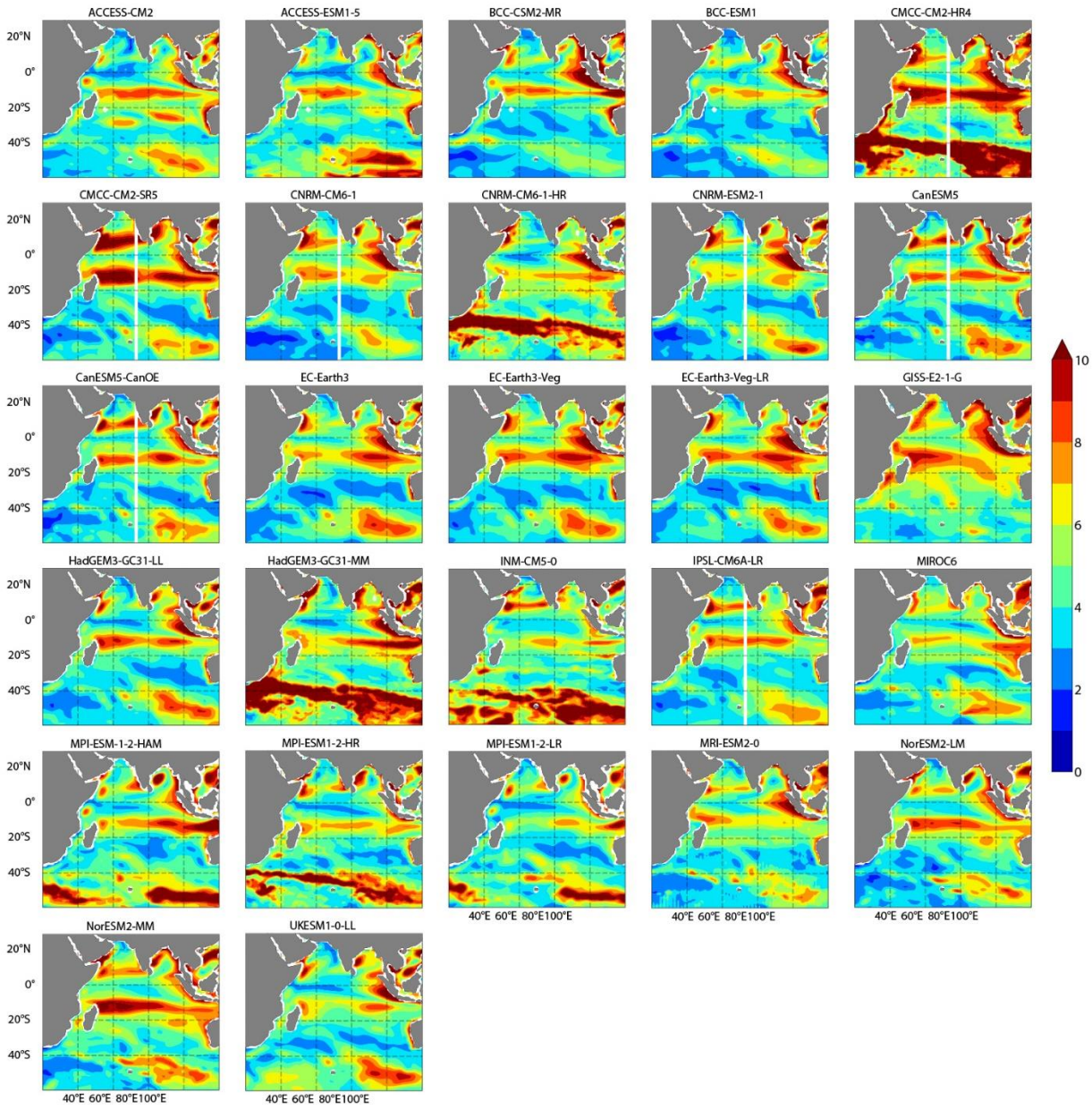

Figure S2: Total standard deviation (cm) of individual CMIP6 models.

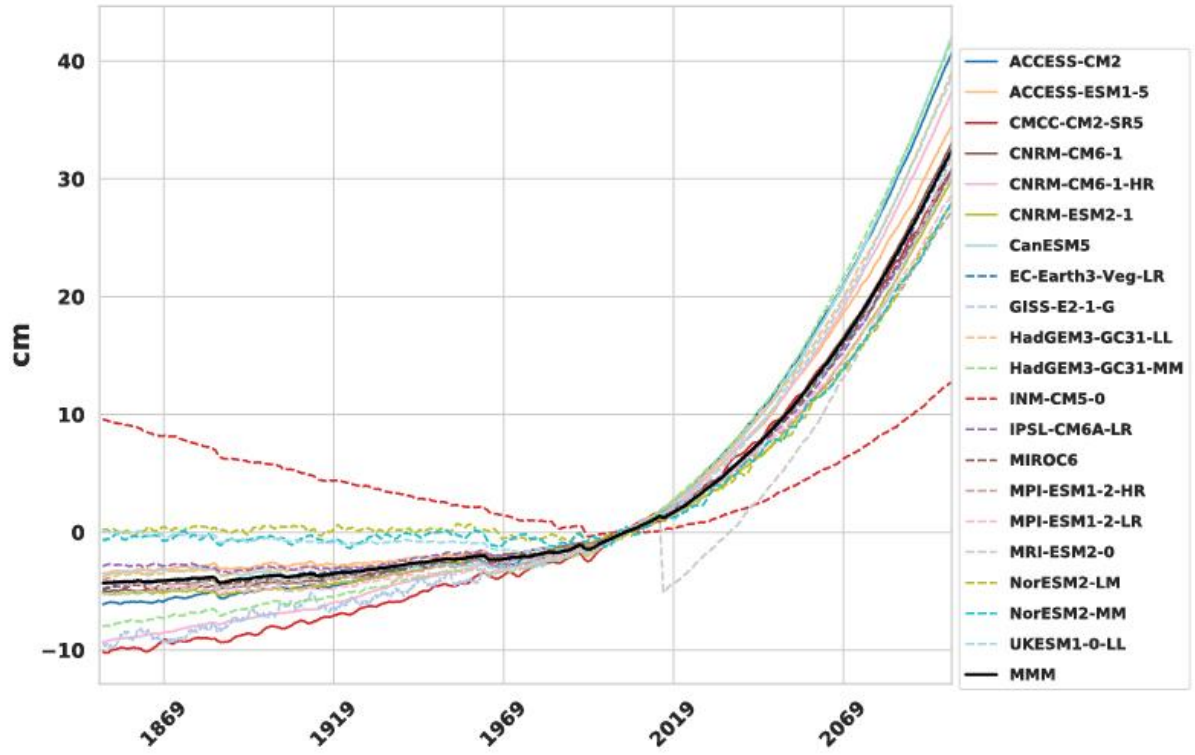

Figure S3: Timeseries of zostoga from all the CMIP6 models.